Cross sections, angular distributions, and magnetic substate populations in the $^{23}Na(n,n'\gamma)$ reaction*

D. R. Donati, S. C. Mathur, E. Sheldon, B. K. Barnes, L. E. Beghian, P. Harihar, G. H. R. Kegel, and W. A. Schier

Department of Physics and Applied Physics, University of Lowell, Lowell, Massachusetts 01854

(Received 8 November 1976; revised manuscript received 16 February 1977)

Neutron inelastic scattering cross sections have been determined for six levels in ^{23}Na over the incident neutron energy range 0.52 to 4.23 MeV by measuring the γ-ray production cross sections for 10 deexcitation γ transitions in the $^{23}Na(n,n'\gamma)$ reaction. γ-ray angular distributions from the first two excited levels were obtained at various incident neutron energies. From these, the magnetic substate populations were evaluated for the 0.440-MeV $(5/2^+)$ first excited level and the 2.078-MeV $(7/2^+)$ second excited level in ^{23}Na. Comparisons have been made between the distributions and magnetic substate populations calculated from compound-nuclear and direct-interaction theory, the former yielding better agreement in the interpretation of experimental results.

[NUCLEAR REACTIONS $^{23}Na(n,n'\gamma)$, $E_n = 0.52$–4.23 MeV; measured $\sigma(E_n,\theta_\gamma)$; deduced $\sigma(E_n)$ and magnetic substate populations; calculated $\sigma(E_n,\theta_\gamma)$, $\sigma(E_n)$, magnetic substate populations; CN and DWBA analysis; natural (Na) target.]

I. INTRODUCTION

The study of neutron scattering by ^{23}Na, the lightest member of the decuplet of target nuclei (Na, Si, Ti, V, Cr, Mn, Fe, Co, Ni, and U) studied by the Lowell group,[1] has provided informative data and insights into current technological, experimental and theoretical considerations of neutron scattering. The study covers the incident energy range $E_n = 0.52$ to 4.23 MeV and scattering angles between 25° and 150°. Increasing attention is being devoted to sodium as a material featured in neutron-induced energy production processes.

As natural sodium is 100% ^{23}Na and is readily available in a chemically pure state for target preparation, problems arising from isotopic impurities are obviated. Moreover, not only is its interaction with neutrons of value in its own right, but the use of neutrons as projectiles avoids the Coulomb-barrier inhibition of threshold measurements and has the advantage over proton projectiles that the latter initiate a $^{23}Na(p,\alpha\gamma)^{20}Ne$ reaction in competition with the scattering process $[Q(p,\alpha) = 2.379$ MeV] that gives rise to intense 1.63-MeV γ radiation from the deexcitation of the first level in ^{20}Ne, which seriously interferes with the measurement of γ-ray transitions in ^{23}Na having comparable energy.

Sodium is of especial technological significance in the development of liquid-metal fast breeder reactors (LMFBR) which are presently being intensively developed. A detailed and reliable knowledge of the interaction characteristics of the $^{23}Na + n$ system as a function of neutron energy is required. Currently the sole breeder reactor to have reached full operational status is the 250-MW plant PHENIX in France, while in the United States at Clinch River, Tennessee and in several other countries similar power-generating reactors are in an advanced stage of planning and construction. In their design, liquid sodium is regarded as a viable coolant,[2] capable of adding to the reactivity of the reactor.[3] Thus for nuclear engineering and energy-production purposes, the acquisition of highly reliable data becomes of paramount urgency toward economic and technically feasible operation.

From an experimental standpoint, the advantages already indicated for the $Na + n$ system are further enhanced by the simplicity of the level scheme for ^{23}Na, as shown in Fig. 1, and by the presence of prominent, distinctive γ-ray transitions that allow of clear identification. The Q values for competing neutron-induced reactions are highly negative, and so effectively filter out all outgoing channels other than those for elastic and inelastic neutron scattering [in particular, (n,p) and (n,α) reactions are thereby precluded, since $Q = -3.597$ and -3.867 MeV, respectively].

Various theoretical aspects invite special attention. It is of particular interest to establish the extent to which a compound-scattering statistical formulation[4] of the Wolfenstein-Hauser-Feshbach type,[5] designed to apply to nuclei beyond $A \simeq 40$, as reviewed in Refs. 6 and 7, nevertheless remains applicable in the case of an $A = 23$ nucleus. In particular we wish to probe the validity of the theory of population of magnetic substates over a range

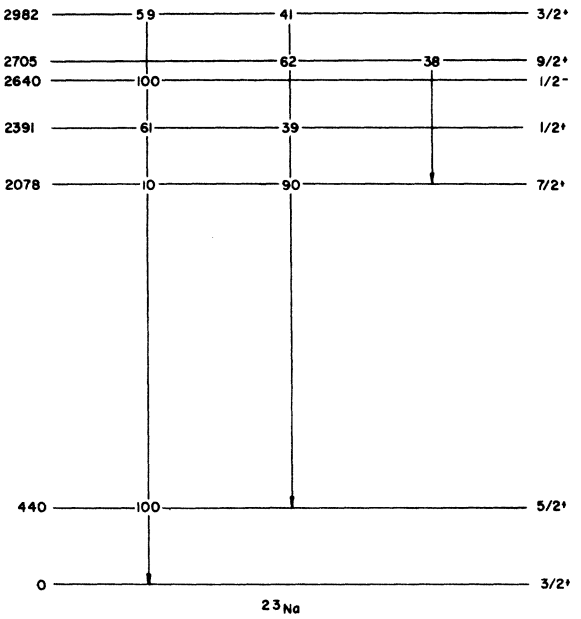

FIG. 1. Energy level scheme for ^{23}Na, showing γ-ray transitions and branching ratios observed in the present investigation.

of incident energies—a hitherto unexplored facet. If nuclear calculations are to have predictive validity in engineering applications, a sensitive test of the formalisms can aid vastly in an assessment of practical problems.

Although, especially of late, data acquisition and interpretation of the Na+n interaction have received considerable attention, previous $(n,n'\gamma)$ studies[8-10] had only in part been concerned with the present important energy region $E_n = 0.52 - 4.23$ MeV (lab), and latterly the focus of study has shifted to higher energies, as in the results published by Lachkar, Patin, and Sigaud[11] for 6.3 – 8.8 MeV. Moreover, ^{23}Na has up to the present been featured more in charged-particle studies than in neutron-induced interactions, as in early (p,γ), $(p,\alpha\gamma)$, $(t,\alpha\gamma)$, and $(\alpha,\alpha'\gamma)$ investigations by various groups[12-16] and in the exploration of high-spin states of ^{23}Na as a residual nucleus in a range of heavy-ion processes, such as the ^{11}B(^{16}O, α)^{23}Na reaction,[17] the ^{12}C(^{12}C, $p\gamma$)^{23}Na reaction,[18,19] and the ^{12}C(^{15}N, α)^{23}Na reaction.[20] The present report aims to consolidate preliminary brief presentations at a number of past conferences[21-23] in which the diverse aspects of this work were described.

II. OVERVIEW OF THE PRESENT INVESTIGATION

In the present study differential γ-ray production cross sections, including excitation functions, were determined from measured data for ten γ-ray transitions observed in the ^{23}Na$(n,n'\gamma)^{23}$Na reaction over the incident energy range from 0.52 to 4.23 MeV (lab).

Angular distributions of 440-keV γ radiation ensuing from the deexcitation of the first excited state have been measured at ten incident neutron energies ranging from 0.73 to 3.82 MeV and corresponding to on-resonance and off-resonance points along the excitation function. Similarly, angular distribution measurements were performed at four incident neutron energies from 2.67 to 3.82 MeV on the 1638-keV γ radiation ensuing from the decay of the second excited state to the first level. The results were in acceptable agreement with Hauser-Feshbach statistical compound-nuclear (CN) theory and furnished information on the relative population of magnetic substates making up the first two excited states of ^{23}Na, viz., at 0.440 MeV ($\frac{5}{2}^+$) and 2.078 MeV ($\frac{7}{2}^+$). A marked change in the distributions and hence in the populations with incident energy was discernible within this range, being particularly pronounced in the vicinity of the threshold in the case of the $\frac{7}{2}^+ \rightarrow \frac{5}{2}^+$ $\gamma_{2,1}$ transition.

In Sec. III we describe the experimental arrangements and procedures employed in the measurements, while Sec. IV is devoted to a discusssion of the data acquisition and analyses. The results are presented in Sec. V and in particular some systematic features are deduced and compared to findings for other compatible reactions by way of shedding light on substate feeding characteristics, which are examined in Sec. VI, and on the extensibility of statistical theory to light nuclei under nonideal conditions.

III. EXPERIMENTAL PROCEDURES

A 5.5-MeV HVEC model CN Van de Graaff accelerator in the Nuclear Center of the University of Lowell was employed to provide a pulsed beam of protons directed onto a neutron-producing target of either tritium or lithium. The lithium target was used for production of neutrons having energies from 0.52 to 0.94 MeV and an energy spread of less than 60 keV in this range. The tritium target was utilized to produce neutrons in the energy range 1.0 to 4.2 MeV having a spread that varied from about 130 keV at 1.0 MeV to about 40 keV at 4.0 MeV.

The sodium scatterer was cylindrical in shape, measuring 5.25 cm in height and 3.33 cm in diameter. The density of the sample was 0.963 g/cm^3. Since ^{23}Na oxidizes rapidly in air and reacts explosively with water, the scatterer was covered with a thin film of oil and housed in three sheaths of thin rubber. The sodium sample was positioned

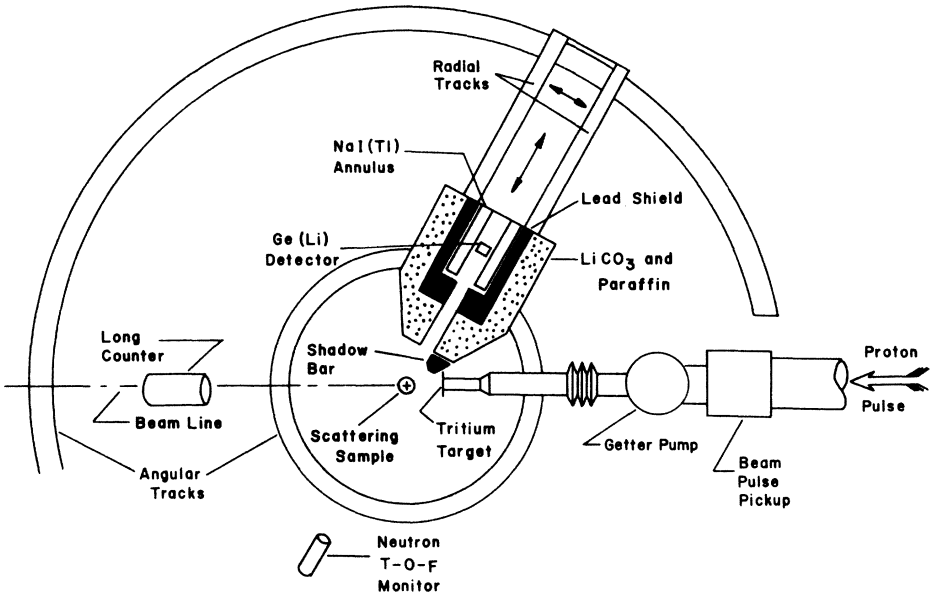

FIG. 2. Geometrical configuration in the $^{23}Na(n,n'\gamma)$ experimental investigations of the angular distribution $\sigma(E_n,\theta_\gamma)$.

11.4 cm from the neutron source.

The γ-ray detector assembly was placed on a support which rode on circular tracks centered on the sample position. In addition to this preprogrammed angular freedom, the support had radial freedom and could be positioned at 50 to 300 cm from the sample. The γ-ray detector consisted of a 40-cm^3 Ge(Li) detector with an active face area of 9.4 cm^2. This assembly was positioned at 57.1 cm and 125° with respect to the sample during the acquisition of the excitation-function data. The complete experimental configuration employed for this experiment is depicted in Fig. 2.

The shielding for the Ge(Li) detector consisted of a 20-cm-long lead tube, a solid copper bar shaped as shown in Fig. 2, measuring 23 cm in length, 7 cm in height, and 7 cm at the widest point, and a main shield constructed of a lithium carbonate and paraffin mixture, 57 cm long, 34 cm wide, and 26 cm high. It should be noted that the experimental setup shown in Fig. 2 is not drawn to scale and that the NaI(Tl) annulus was removed due to interference of sodium γ rays from the annulus.

During the acquisition of each datum point, the neutron flux was continuously monitored by two independent devices. The neutron spectrum was obtained with the aid of a pilot B scintillator optically coupled to a 14-stage RCA photomultiplier placed at 45° and 125 cm with respect to the neutron source. This neutron time-of-flight monitor allowed on-line monitoring of the neutron beam assuring no energy shifts during the acquisition of data and was used to normalize background runs for the long counter. The other monitor was a Hansen and McKibben type long counter.[24,25]

Since the sample was placed between the long counter and the neutron source, the long counter was exposed to a modified neutron flux. Therefore, after each datum point, three short runs, normalized by the neutron time-of-flight monitor, were taken to determine the neutron flux viewed by the sample: one in the original geometry to verify consistency of the experimental conditions; the second with the sample removed to allow the long counter to sample the 0° neutron flux as seen by the sample; the third with a 55-cm-long and 22-cm-diam cone of paraffin, lithium carbonate and iron placed between the long counter and neutron source to determine the effect of background radiation on the long counter.

The long counter was calibrated using a proton recoil counter[25,26] which consisted of a surface barrier detector viewing a thin polyethylene radiator with defining apertures of tantalum. The experimental error involved in this calibration was 6% for any given datum point above $E_n = 2.3$ MeV: it increased to $7\frac{1}{2}-8$% for lower energy points because the long counter was positioned at back angles to the beam. This calibration is shown in Fig. 3, where the units are neutrons per long counter count and per steradian. The electronic circuitry associated with these two neutron monitors is depicted in Fig. 4.

Time gating of the γ-ray spectrum was utilized to reduce the amount of background radiation

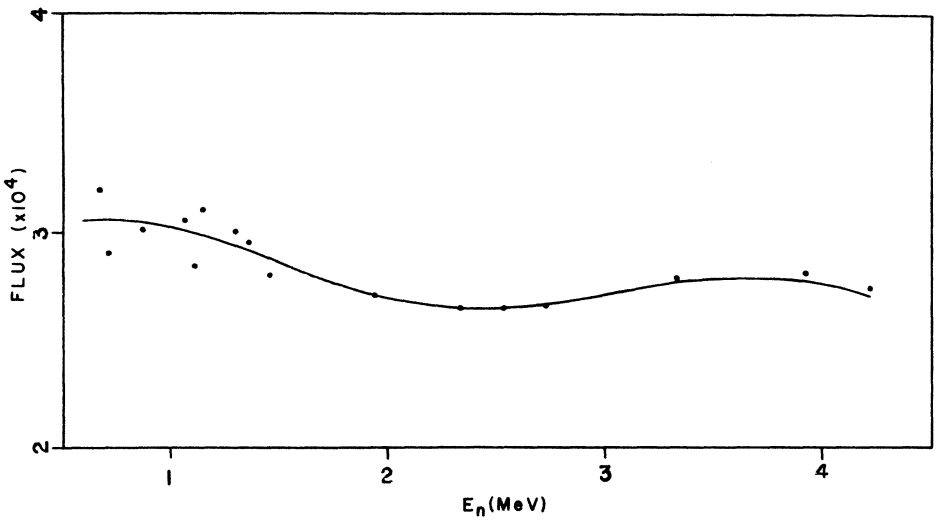

FIG. 3. Long counter calibration as a function of impinging neutron energy in the laboratory system.

counts. The electronic circuitry used for the acquisition of the γ-ray spectrum and the time gating is schematized in Fig. 5. A typical gated and ungated Ge(Li) time spectrum is indicated in Fig. 6, where the time scale is 0.385 ns/channel and E_n = 3.5 MeV.

After gating, the γ-ray energy signal was sent to the amplitude-to-digital converter (ADC) on an on-line PDP-9 computer. The computer program JOANIE[28] was used to collect the data from the ADC and store the results in core memory in order to allow the experimenter to carry out preliminary analysis of the data while in process of acquisition. After a spectrum had been obtained, it was stored on a magnetic tape from which the spectrum could be regenerated for further analysis.

The efficiency of the Ge(Li) detector and its associated electronics was experimentally determined, using calibrated γ-ray sources. The entire Ge(Li) circuitry was employed in measuring the efficiency because the extrapolated zero strobe reduces low-energy efficiency, and time gating reduces the overall efficiency, as a consequence of dead time in the circuitry. A log-log plot of the efficiency is presented in Fig. 7. The efficiency ranged from 40% at 200 keV to 2% at 3 MeV.

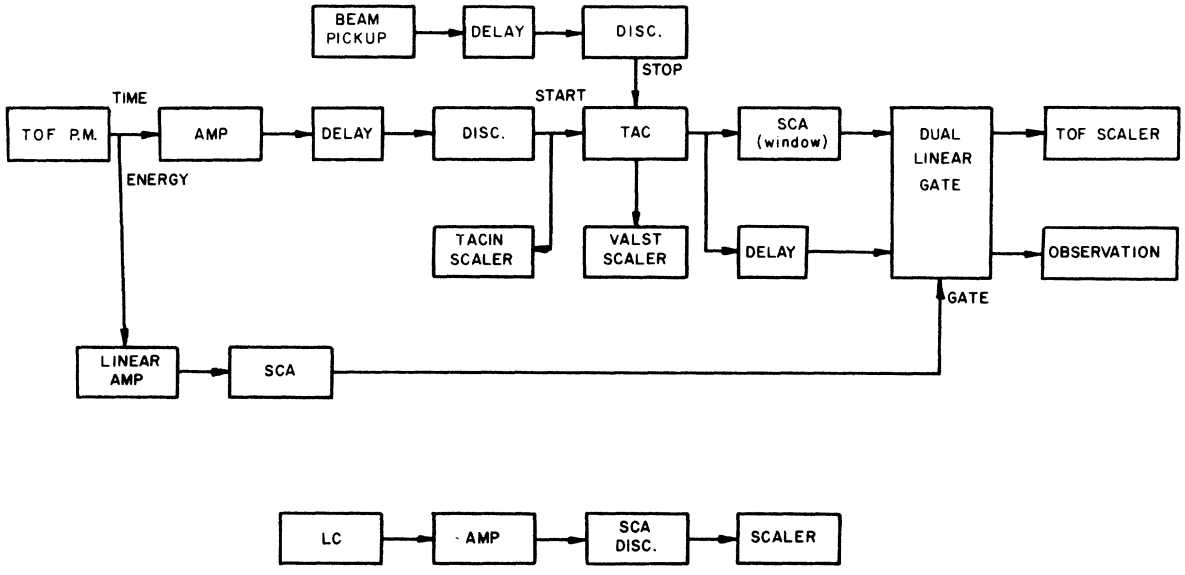

FIG. 4. Block diagram of the neutron time-of-flight (TOF) and long counter (LC) monitors.

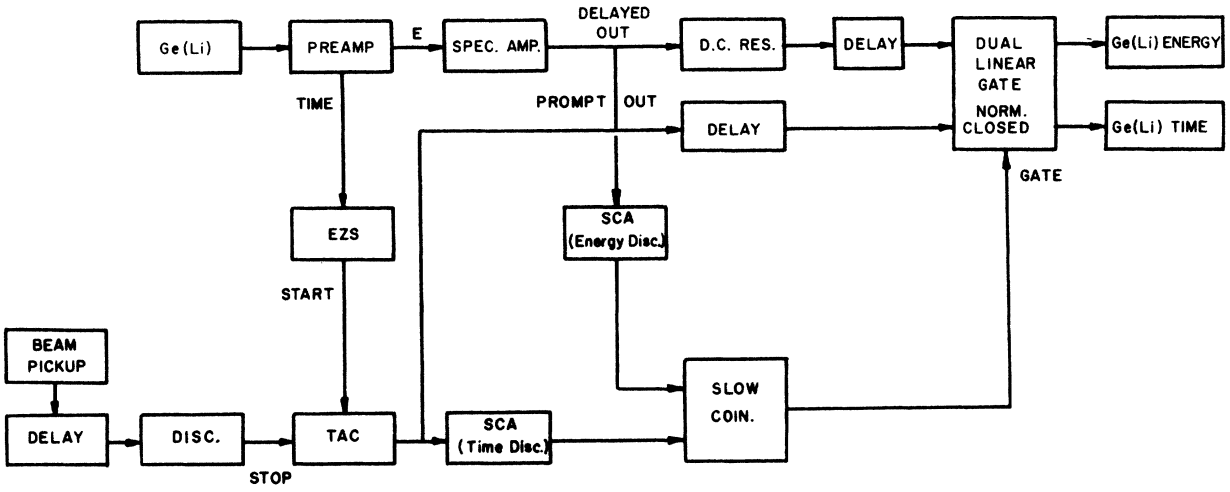

FIG. 5. Block diagram of the electronics of Ge(Li) detector time gating.

IV. NEUTRON EXCITATION FUNCTIONS

From the γ-ray energy spectra, the yields of 10 γ transitions in ^{23}Na could be derived by using the computer program GASPAN.[27-31] The differential γ-ray production cross sections were evaluated from these yields on substituting numerical values of the incident neutron flux, the Ge(Li) efficiency, sample size and corrections for neutron flux attenuation, neutron multiple scattering, and γ-ray attenuation within the sample. Cascade corrections were made to the γ-ray yields and the angle-integrated cross sections were derived by multiplying the 125° differential cross sections by 4π.

The results are presented in Figs. 8 to 13 as plots of the neutron excitation functions for the first six excited states in ^{23}Na. The plotted error bars represent absolute uncertainties. The solid curves in these figures were generated by Hauser-Feshbach calculations[4,5,7] undertaken with the com-

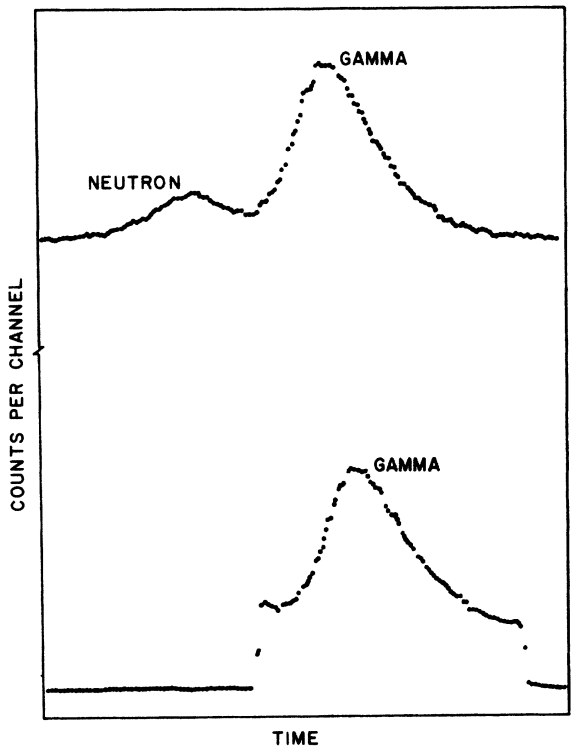

FIG. 6. Ungated and gated Ge(Li) detector time spectra.

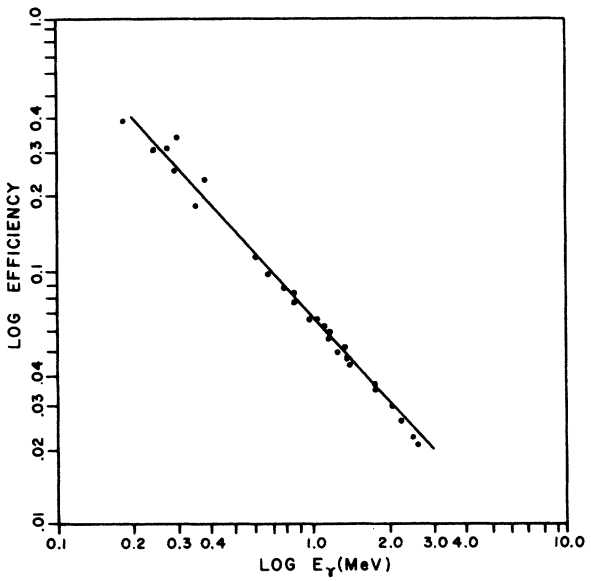

FIG. 7. Log-log fit of Ge(Li) detector efficiency as a function of γ-ray energy.

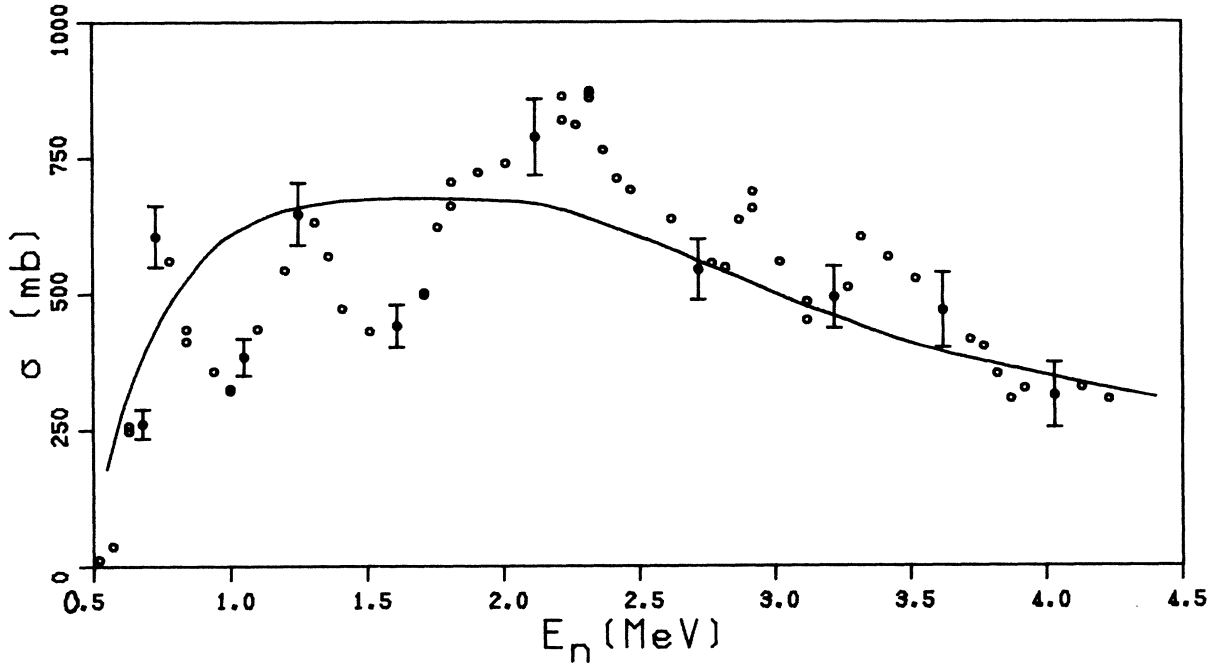

FIG. 8. Experimental (dots, with statistical error bars) and CN theoretical (solid curve) neutron excitation functions for the 440-keV ($\frac{5}{2}^+$) first level in ^{23}Na.

puter code MANDYF.[32,33]

The optical-model potentials used in evaluating the transmission coefficients for neutrons on ^{23}Na were of the customary Woods-Saxon type with surface absorption (W-S derivative form factor) plus a real spin-orbit term of the Thomas form,

$$V(r) = V_{re}(r) + iV_{im}(r) + V_{so}(r)\,, \tag{1}$$

$$V_{re}(r) = -\frac{V}{1+\exp[(r-R)/a]}\,, \tag{2}$$

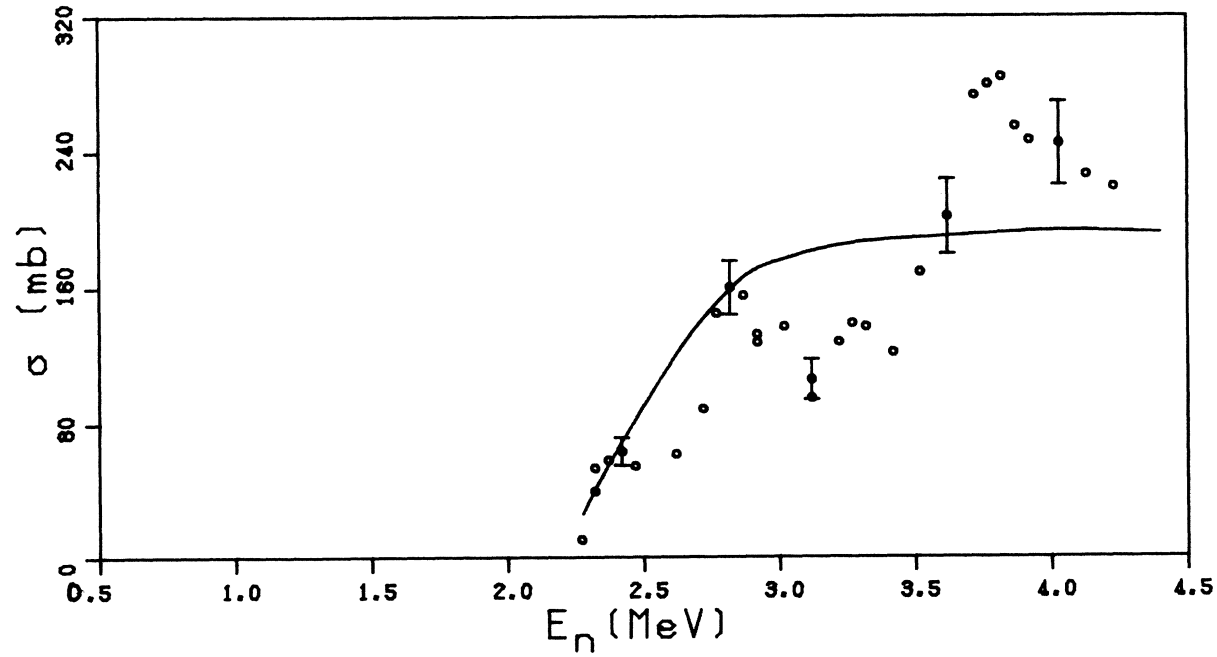

FIG. 9. The same as Fig. 8, but for the 2078-keV ($\frac{7}{2}^+$) second level in ^{23}Na.

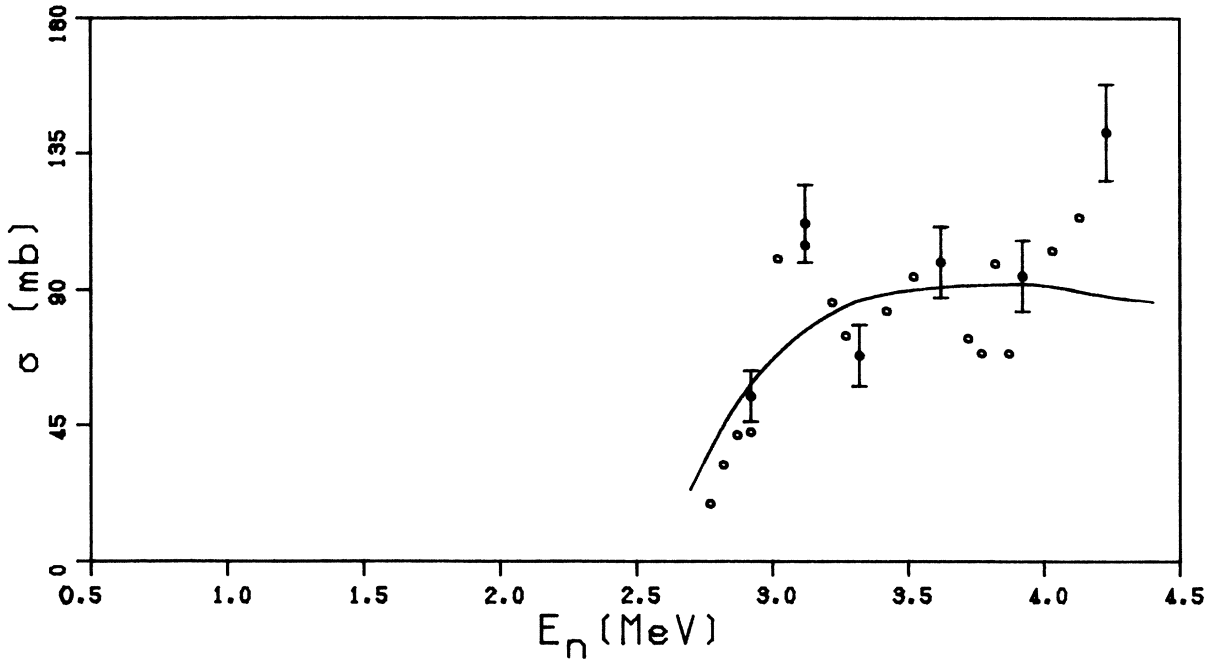

FIG. 10. The same as Fig. 8, but for the 2391-keV ($\frac{1}{2}^+$) third level in ^{23}Na.

$$V_{\mathrm{im}}(r) = -\frac{4bW\exp[(r-R')/b]}{\{1+\exp[(r-R')/b]\}^2}, \tag{3}$$

$$V_{\mathrm{so}}(r) = -(\hbar/m_\pi c)^2 V_s \frac{1}{r}\left[\frac{d}{dr} V_{\mathrm{re}}(r)\right](\vec{\mathrm{L}}\cdot\vec{\mathrm{S}}). \tag{4}$$

The parameters used within these expressions were established by Chien and Smith[34] through fits of energy-averaged elastic-scattering data for ^{23}Na+n, and are V=46.0 MeV, W=6.0 MeV, V_s =6.0 MeV, $R=R'$=4.0 fm, a=0.3 fm, and b=0.7

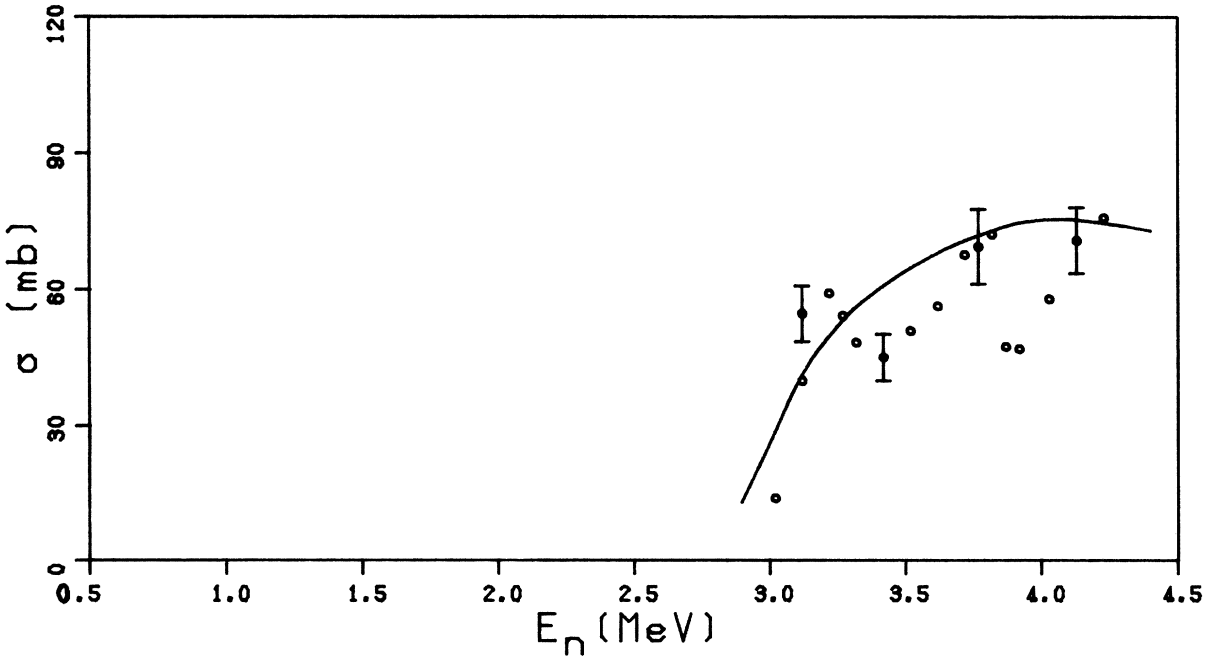

FIG. 11. The same as Fig. 8, but for the 2640-keV ($\frac{1}{2}^-$) fourth level in ^{23}Na.

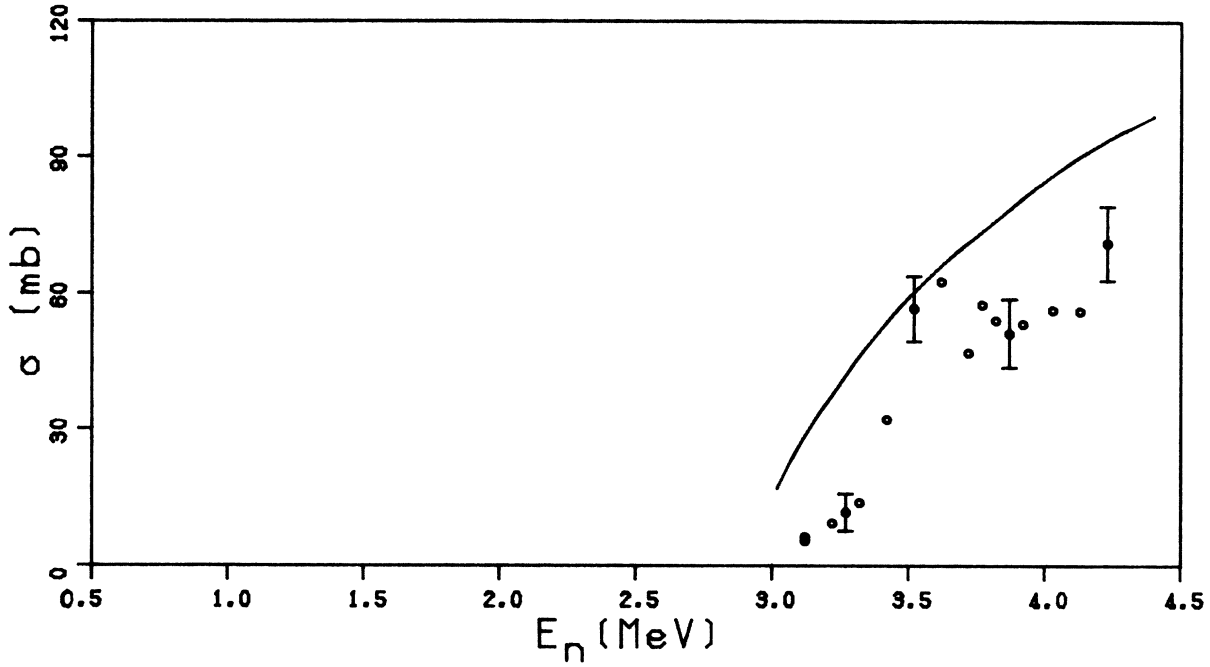

FIG. 12. The same as Fig. 8, but for the 2705-keV ($\frac{9}{2}^+$) fifth level in ^{23}Na.

fm.

As is obvious from the plots, this theoretical approach cannot be expected to reproduce the detailed structure of the resonances that are evident in the measured excitation functions, but this is a common finding even in the case of heavier nuclei at these comparatively low incident energies. What is remarkable, and rather gratifying, is that despite the nonfulfillment of the statistical assumption, the general trends of the data are fitted so

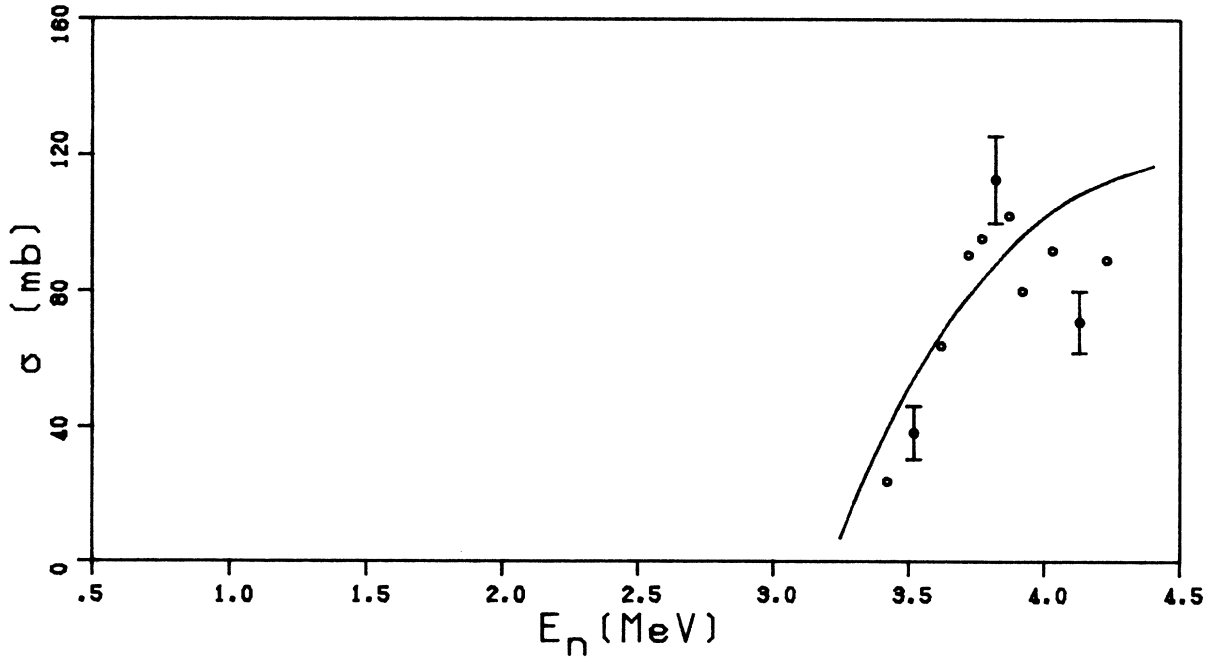

FIG. 13. The same as Fig. 8, but for the 2982-keV ($\frac{3}{2}^+$) sixth level in ^{23}Na.

well. At the higher excitation energies where the level density begins to approach the prerequisite for validity of the statistical quasicontinuum assumption the agreement is particularly good, but it is noteworthy that even in the vicinity of the threshold with such a light target nucleus it is possible for Hauser-Feshbach theory to render such a good account of the experimental findings. Although angular distribution data are basically less likely to be sensitive to inadequacies in the continuum assumption than are corresponding angular-correlation or polarization-correlation data, and even bearing in mind the circumstance that excitation functions are likely to be even less sensitive inasmuch as they tap only a segment of the whole angular distribution, it is remarkable not so much that it is done well, but that it is done at all.

The results thus offer the decisive hope that theoretical calculations might well be in a position to render a quite acceptable account of the variation of cross section with energy (and angle) even when level conditions might seem to jeopardise this.

The neutron excitation function for the 440-keV level, shown in Fig. 8, accounts for 100% of the total inelastic neutron scattering cross section below an incident neutron energy of 2.22 MeV (lab), and decreases in relative magnitude to 33% of the total inelastic cross section at $E_n = 4.23$ MeV (lab).

Several prominent resonances appear in this excitation function, the sharpest of which occurs at $E_n = 0.73$ MeV. However, it is not a pure resonance: in point of fact 73 resonances have been reported[35] in the incident neutron energy range 0.63 to 0.83 MeV.

The neutron excitation functions for the 440-, 2078-, and 2391-keV levels all peak, with a pronounced resonance at 1.6 to 1.7 MeV above threshold. The remaining neutron excitation functions also contain resonance structure, but did not attain a maximum within the energy range considered.

V. ANGULAR DISTRIBUTIONS

Angular distributions of the 440-keV γ-ray transition were determined between 25° and 140° at 10 incident neutron energies corresponding to points on and off the resonances in the excitation function. They are illustrated in Figs. 14 to 18. Angular distributions of the 1638-keV γ radiation from the second to the first level were taken at four incident neutron energies and are shown in Figs. 19 and 20. The angular distributions were corrected for cascade effects and angle dependent corrections were made for multiple scattering and γ-ray attenuation. The statistical error in reducing the raw data, represented by the plotted error bars, ranged from less than 1% for high yield datum points to 13% for low yield datum points. The solid curve is an even-order Legendre-polynomial fit to the experimental data by the method of least squares. The broken curve in some figures is the prediction of direct-interaction (DI) theory, as evaluated from the computer program DWUCK[36] at neighboring incident energies; the crosses represent the theoretical prediction of the angular distribution using Hauser-Feshbach-Satchler formalisms[7,4] (devoid of Moldauer level-width

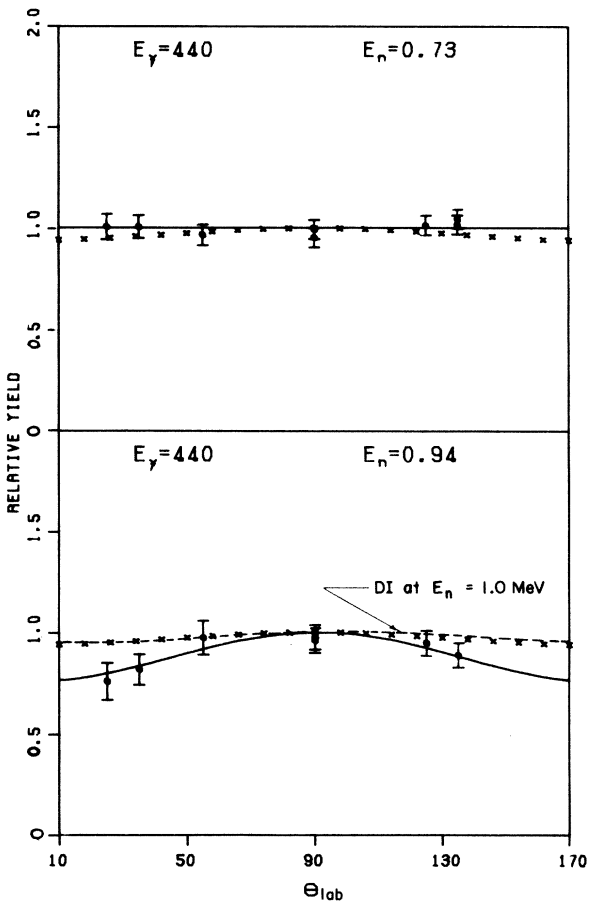

FIG. 14. Angular distributions for the 440-keV γ-radiation transition ($\frac{5}{2}^+ \rightarrow \frac{3}{2}^+$) deexciting the first level of ^{23}Na following the inelastic scattering of neutrons at $E_n = 0.73$ and 0.94 MeV (lab). All resuts are normalized to unity at 90°. The points (and statistical error bars) depict experimental values after correction for detector efficiency and finite sample size. The least-squares Legendre-polynomial fit to these points is indicated by the solid curve, and the predictions of DWBA direct-interaction theory by the broken curve. The crosses mark the values provided by statistical compound-nuclear scattering theory. Note that the angular range extends from 10° to 170°. The multipole mixing ratio is $\delta = +0.08$.

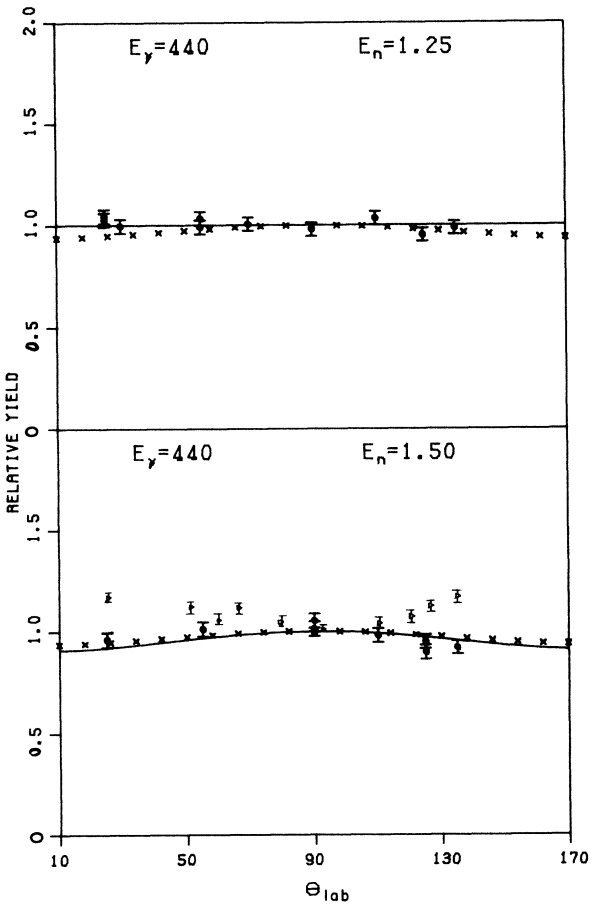

FIG. 15. The same as Fig. 14, but for $E_n = 1.25$ and 1.50 MeV. The triangles denote experimental results by Towle and Gilboy (Ref. 10), at variance with the present findings.

fluctuation effects). The $M1/E2$ multipole mixing ratios used in these calculations were $\delta(440) = +0.08$ and $\delta(1638) = +0.18$, as determined by Poletti *et al.*,[13,14] which are in good agreement with the respective values $\delta(440) = +0.09$ and $\delta(1638) = +0.22$ cited by Lindgren *et al.*[15] (we employ the Biedenharn-Rose[37] sign convention for the amplitude ratio $\delta \equiv E2/M1$, which in this case is opposite in sign to the Rose-Brink[38] convention used by the above authors). Table I lists the Legendre coefficients so obtained for the experimental fits and the theoretical CN and DI curves. Experimental results for the 440-keV γ distribution at $E_n = 1.50$ MeV by Towle and Gilboy[10] are shown in Fig. 15 and discussed in Sec. VII.

A comparison of the 440-keV γ-ray angular distributions with CN theory indicates that the theoretical distributions remain essentially constant while the experimental distributions fluctuate in the vicinity of the first two resonances and then exhibit increasing anisotropy as a function of increasing excitation energy. The latter effect may be due to increasing direct-interaction involvement. Attempts to evaluate the DI influence with the distorted-wave Born-approximation (DWBA) codes DRC[37] and JULIE[40,41] by the present group ran into computational difficulties, but some independent calculations at neighboring energies have been performed by Rogers,[42] using the code DWUCK.[36] His findings of a practically isotropic DI angular distribution for the deexcitation γ transition from the first level (namely, 6% anisotropy at $E_n = 1$ MeV, peaking symmetrically at 90°, and effectively 0% anisotropy at $E_n = 4$ MeV) render this interpretation rather dubious.

The DWUCK output for the 1638-keV γ distribution again effectively indicates isotropy over the entire energy range [the ratio of $W(0°)/W(90°)$ being 1.011]. The CN predictions are likewise essentially isotropic over this energy range, the anisotropy ratio being $W(0°)/W(90°) = 1.013$. The experimental γ-distribution data at $E_n = 2.67$, 2.87, 3.62, and 3.82 MeV can also within error limits be regarded as effectively isotropic, in good agree-

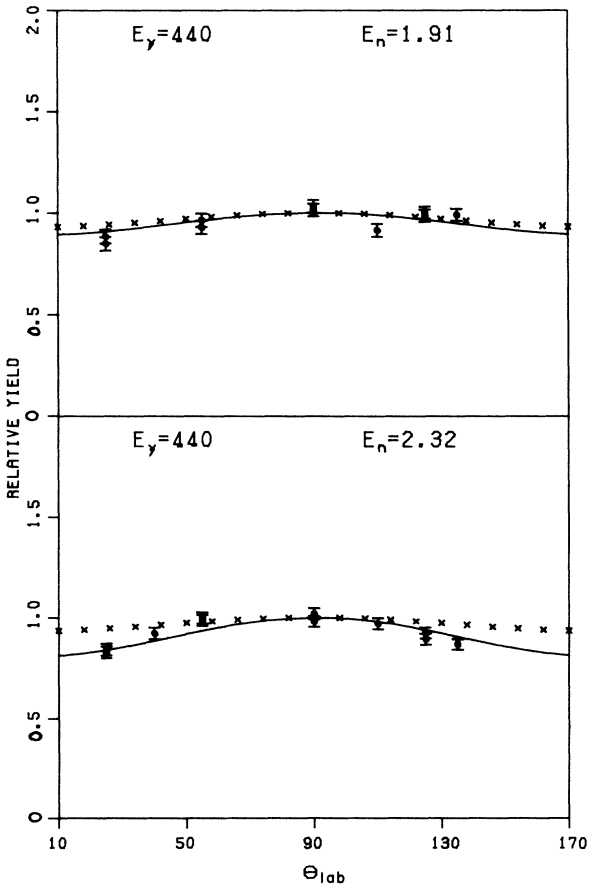

FIG. 16. The same as Fig. 14, but for $E_n = 1.91$ and 2.32 MeV.

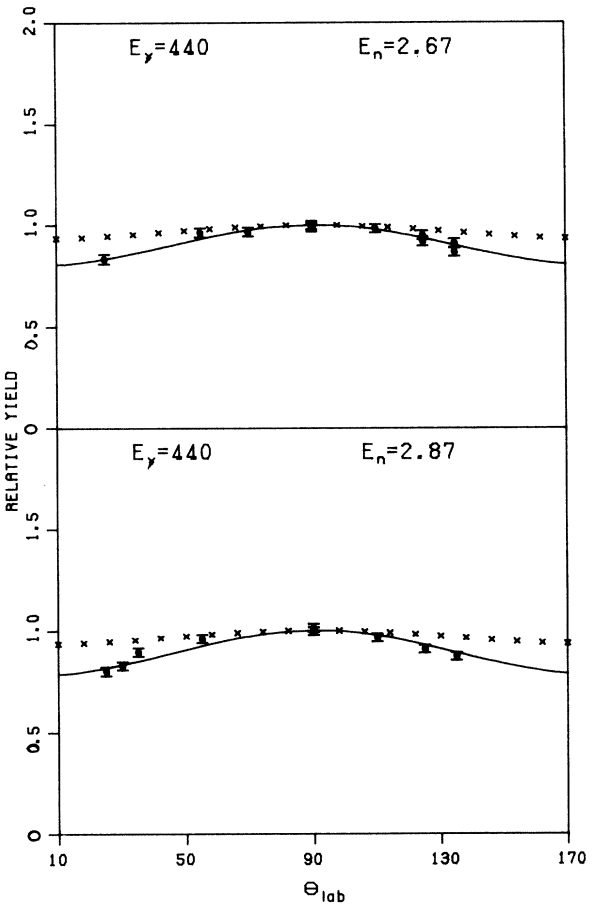

FIG. 17. The same as Fig. 14, but for $E_n = 2.67$ and 2.87 MeV.

ment with CN theory, as can be seen from Figs. 19 and 20. Therein, the apparent indication of slight structure, changing from W- or U-shaped curvature with respect to the abscissa at the lower energies to the onset of concavity (i.e., bell-shaped structure) at the uppermost energy, is almost certainly misleading. Such seeming undulations would occasion Legendre least-squares-fit coefficients of considerably larger magnitude (and of opposite sign in the case of the γ distribution at $E_n = 3.82$ MeV) when compared, as in Table I, with the small values predicted by CN (or DI) theory, or with the zero values that would correspond to exact isotropy. The least-squares fitting procedure that provides these comparatively large Legendre-fit coefficients yields an angular dependence that is shown as solid undulating curves in Figs. 19 and 20 which tend to give exaggerated prominence to the seeming departure from isotropy.

Additional support for the contention that within the indicated error limits the data conform to near isotropy as furnished by CN theory accrues from the finding that insertion of the "best-fit" Legendre coefficients into the procedure for evaluating relative magnetic substate populations, as described in the next section, not only yields "experimental" values of population parameters that stand drastically at variance with the theoretical predictions but in fact give rise to evidently nonphysical values, which in certain instances run into the negative domain. Specifically, one finds from these best-fit Legendre coefficients, the following relative substate populations:

$P(M)$ ratios

$$\equiv P(\tfrac{1}{2})/P(\tfrac{3}{2})/P(\tfrac{5}{2})/P(\tfrac{7}{2})$$

$$= 264\%/56\%/-182\%/-89\% \text{ at } E_n = 2.67 \text{ MeV}$$

$$= 131\%/24\%/-91\%/-14\% \text{ at } E_n = 2.87 \text{ MeV}$$

$$= 128\%/76\%/-19\%/-135\% \text{ at } E_n = 3.62 \text{ MeV}$$

$$= -146\%/-11\%/140\%/67\% \text{ at } E_n = 3.82 \text{ MeV}.$$

These values were derived using a multipole mixing ratio of $\delta = +0.18$ for the 1638-keV γ transition

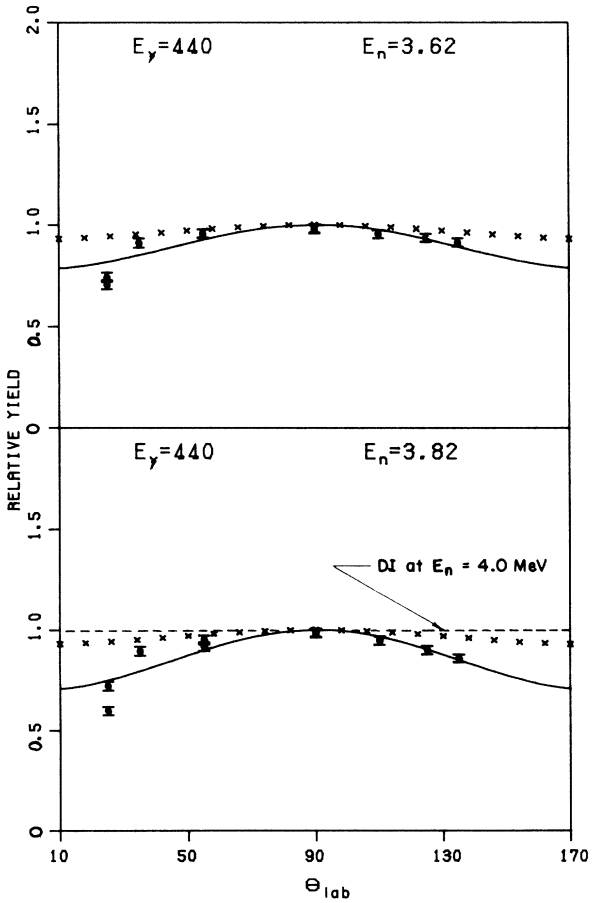

FIG. 18. The same as Fig. 14, but for $E_n = 3.62$ and 3.82 MeV.

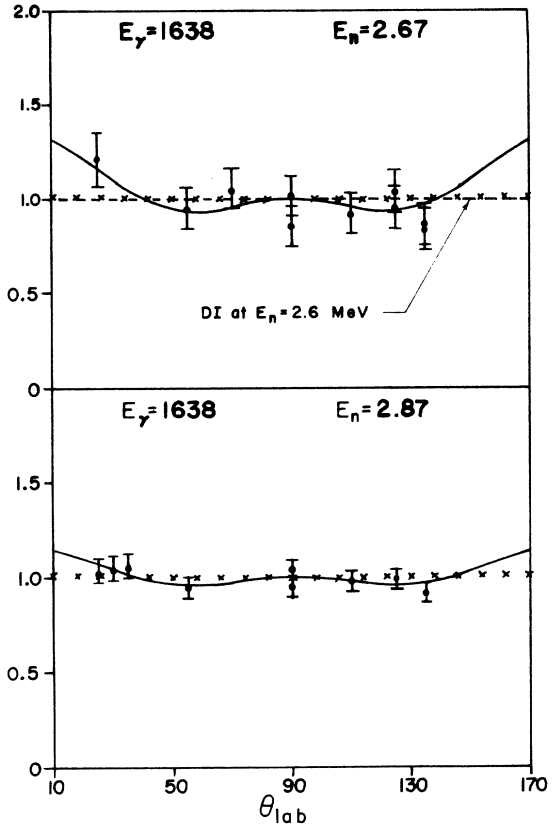

FIG. 19. Angular distribution results as in Fig. 14, but for the 1638-keV γ_{21} transition from the 2078-keV ($\frac{7}{2}^+$) second level to the 440-keV ($\frac{5}{2}^+$) first level in ^{23}Na, following inelastic scattering of neutrons at $E_n = 2.67$ and 2.87 MeV. The multipole mixing ratio is $\delta = +0.18$. The CN and DI predictions are both essentially isotropic.

from the $\frac{7}{2}^+$ (2.038 MeV) level (and are not significantly improved by using $\delta = +0.22$ instead). Thus, magnetic-substate evaluations provide an additional, and very sensitive, means of relating experiment to theory along lines discussed in the next section, and support the conclusion that a CN interpretation is able to match the data within error limits, subject to shortcomings in the statistical quasicontinuum assumption.

VI. MAGNETIC SUBSTATE POPULATIONS

Any nuclear scattering or interaction process differentially populates the magnetic sublevels M that make up the residual nuclear state of spin J (where $M = -J, -J+1, \ldots, J-1, J$). The underlying theory to evaluate the relative population of each substate in an ensemble is based on the Devons-Goldfarb distribution formalism[43] in the Poletti-Warburton approach,[44] and has been presented explicitly by Sheldon *et al.*[4] in numerical guise suitable for computer treatment.

Basically, in a Legendre-polynomial expansion that describes the distribution shape,

$$W(\theta) = \sum_{\substack{\nu=0 \\ \nu \text{ even}}}^{(2J,\,2J+1)} a_\nu P_\nu(\cos\theta) = 1 + \sum_{\nu=2}^{(2J,\,2J+1)} a_\nu^* P_\nu(\cos\theta), \quad (5)$$

the coefficients $a_\nu^* \equiv a_\nu/a_0$ may be expressed as a product of statistical tensors $\rho_\nu(J)$ and calculable Ferentz-Rosenzweig[45] γ-transition coefficients A_ν, made up of Racah-algebraic F_ν coefficients, viz., $a_\nu^* = \rho_\nu(J) A_\nu Q$ (the γ-attenuation coefficient Q in the theory is unity). In their turn, the statistical tensors $\rho_\nu(J)$ are themselves decomposable into substate tensors $\rho_\nu(J, M)$:

$$\rho_\nu(J) = \sum_{M=-J}^{+J} \rho_\nu(J, M) P(M)$$

$$= \sum_{M=0}^{+J} (2 - \delta_{M0}) \rho_\nu(J, M) P(|M|). \quad (6)$$

In the last equality, use has been made of the fact that there is a symmetry in the population $P(M)$ of the magnetic substates in the sense that $P(+M)$

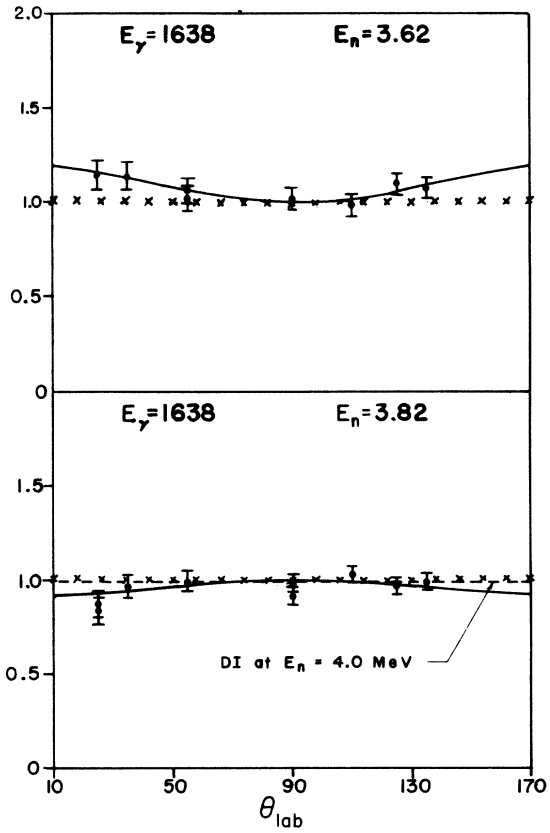

FIG. 20. The same as Fig. 19, but for $E_n = 3.62$ and 3.82 MeV.

TABLE I. Legendre-polynomial coefficients describing the γ-ray angular distributions.

γ-ray energy (keV)	Neutron energy (MeV)	Experimental $a_\nu^* \equiv a_\nu/a_0$ a_2^*	Experimental $a_\nu^* \equiv a_\nu/a_0$ a_4^*	CN theoretical $a_\nu^* \equiv a_\nu/a_0$ a_2^*	CN theoretical $a_\nu^* \equiv a_\nu/a_0$ a_4^*	CN theory a_0 (mb/sr)	DI theory a_2^*	DI theory a_4^*
440	0.73	0	0	−0.04171	-4.261×10^{-5}	44.76		
	0.94	−0.18 ± 0.05	0	−0.04244	-4.401×10^{-5}	50.85	−0.0344	0.00083
	1.25	0	0	−0.04349	-4.442×10^{-5}	53.18		
	1.50[a]	−0.07 ± 0.05	0	−0.04462	-4.356×10^{-5}	53.87		
	1.91	−0.08 ± 0.06	0	−0.04813	-3.211×10^{-5}	53.18		
	2.32	−0.14 ± 0.04	0	−0.04500	-2.627×10^{-5}	46.77		
	2.67	−0.14 ± 0.02	0	−0.04632	-2.433×10^{-5}	41.69		
	2.87	−0.16 ± 0.02	0	−0.04620	-2.524×10^{-5}	37.87		
	3.62	−0.16 ± 0.04	0	−0.04856	-1.813×10^{-5}	29.53		
	3.82	−0.22 ± 0.06	0	−0.05004	-1.091×10^{-5}	26.07	−0.00141	−0.00009
1638	2.67	0.15 ± 0.11	0.18 ± 0.13	0.007749	0.001862	13.63	0.007634	−0.00046
	2.87	0.06 ± 0.03	0.10 ± 0.05	0.007421	0.001544	14.53		
	3.62	0.12 ± 0.03	0.01 ± 0.06	0.007176	0.001339	15.31		
	3.87	−0.09 ± 0.04	−0.12 ± 0.05	0.007140	0.001352	15.36	0.006606	−0.00026

[a] At $E_n = 1.50$ MeV, the experimental 440-keV γ-ray angular distribution obtained by Towle and Gilboy (Ref. 10) is fitted with the Legendre coefficient $a_2^* = 0.14 \pm 0.03$; the authors state that if a $P_4(\cos\theta_\gamma)$ term is included, the coefficient a_4^* is not larger than its error. Note that these findings are at variance with ours above.

$= P(-M)$. The populations are normalized to unity, so that $\sum_M P(M) = 1$ for $M = -J$ to $+J$, and the symbol δ_{M0} denotes a Kronecker δ.

From these relations, each allowed even value of ν from 2 to $\min(2J, 2J+1)$ contributes one equation to a set of simultaneous linear equations expressing the a_ν^* in terms of populations $P(M)$; these can be solved by determinant methods to obtain the individual $P(M)$ in terms of ascending orders of a_ν^* for any given nuclear spin J, and thereby the substate populations determined from (experimental least-squares, or theoretical) a_ν^* data.

The results so derived from the 440-keV γ-transition data are shown in Fig. 21 for the substates $M = \frac{1}{2}, \frac{3}{2}, \frac{5}{2}$ of the $J = \frac{5}{2}$ first excited state. They evince remarkably good agreement between theory (solid curves) and experiment, the relative populations diminishing monotonically with increasing M at any given energy, and remaining comparatively unaffected by a change in energy over the range under consideration. It is, however, discernible that agreement between theory and experiment worsens progressively with increase in incident energy, possibly as a result of inadequacies in the statistical assumption or of an onset of slight direct-interaction contributions. The latter would, however, have to be coherently mixed with the CN amplitudes, as a calculation on the basis of DI theory yields $P(M)$ that do not differ at all appreciably from those provided by CN theory [for example, at $E_n = 4.5$ MeV the DI prediction for the relative populations is $P(\frac{1}{2})/P(\frac{3}{2})/P(\frac{5}{2}) = 22\%/13\%/15\%$, whereas the CN prediction is 20%/18%/12%, and similarly at the low energy end: For $E_n = 0.5$ MeV the respective ratios are 22%/13%/14% for DI, and 19%/18%/13% for CN].

The variation of substate population with energy is more pronounced, especially near threshold, in the case of the 2078-keV($\frac{7}{2}^+$) second excited level, for the 1638-keV γ_{21}-transition data shown in Fig. 22 indicate that the $P(M)$ relative magnitudes remain in a monotonic sequence with increasing M at any given incident energy E_n, but initially vacillate before assuming an effectively constant apportionment, given by

$$P(\tfrac{1}{2})/P(\tfrac{3}{2})/P(\tfrac{5}{2})/P(\tfrac{7}{2}) = 21\%/16\%/9\%/4\%. \qquad (7)$$

This may be compared with the respective DI relative apportionment, viz., 20%/13%/13%/4%. The DI calculations also indicate a similar threshold effect: They yield the values 25%/9%/16%/1% for $E_n = 2.2$ MeV. Unfortunately, the aforementioned discrepancies between experimental (least-squares) and theoretical Legendre coefficients a_ν^* prevents one from deriving sensible $P(M)$ values from the experimental data in this case—the substate population values are too sensitive to slight changes, so that the agreement in Fig. 21 is all the more noteworthy.

It is interesting to observe that the relative apportionment in Eq. (7) corresponds closely to a normalized Gaussian distribution. In a statistical study of nuclear level characteristics, Ericson[46] has considered a Gaussian distribution of M's given by the distribution function

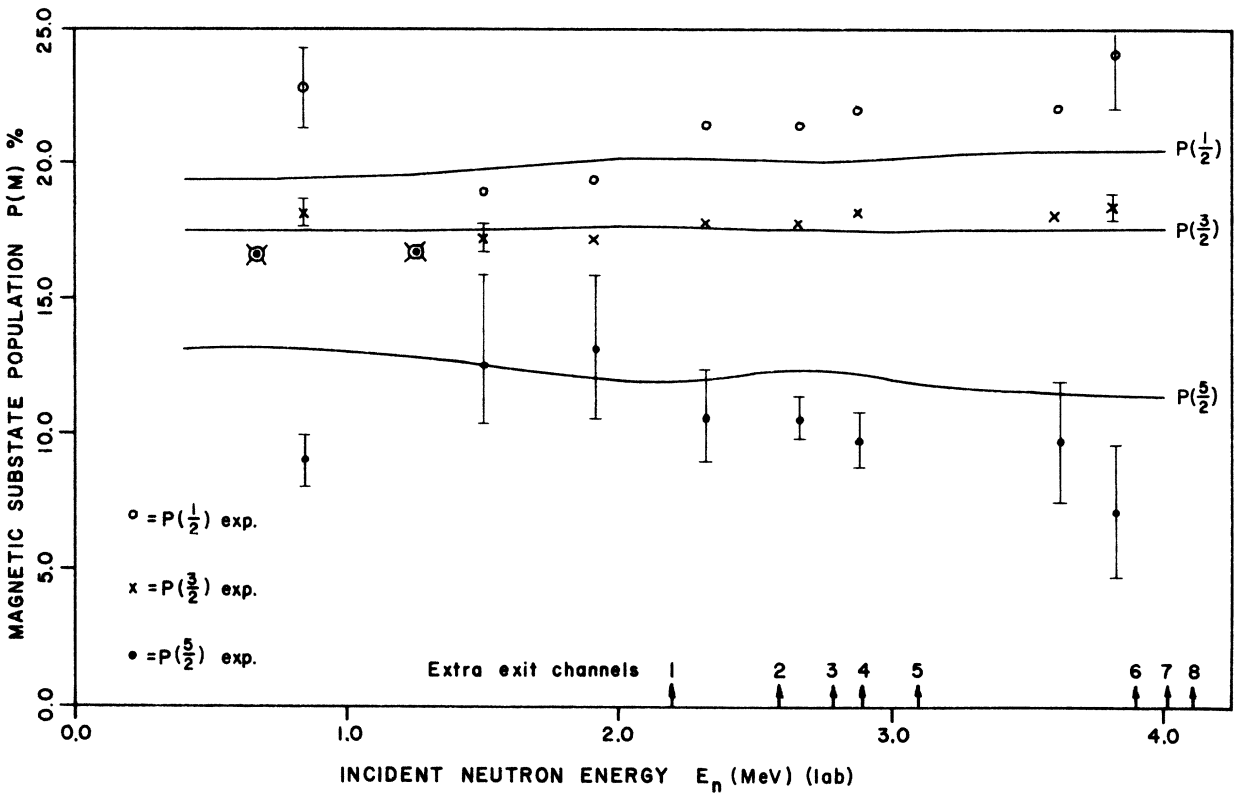

FIG. 21. Experimental and CN theoretical variation with energy of magnetic substate populations $P(M)$ for the 440-keV ($\frac{5}{2}^+$) first level in ^{23}Na, as deduced from Legendre-polynomial coefficients. The entry of competing n' channels with increasing incident energy is indicated at the foot of the diagram. The agreement is remarkably good in view of the sensitiveness of the results toward even minute changes in the Legendre coefficients. Note the monotonic sequence of $P(M)$ with increasing M at any given energy. The distribution of the $P(M)$ is non-Gaussian. The DI predictions, cited in the text, yield poorer agreement.

$$G(M) = (2\pi\sigma^2)^{-1/2} \exp(-M^2/2\sigma^2), \tag{8}$$

where the spin cut-off parameter σ may be taken[47] for ^{23}Na to be $\sigma = 2$. On the basis of this formula, the renormalized relative apportionment of substate populations would be

(a) For $J = \frac{7}{2}$:

$$P(\tfrac{1}{2})/P(\tfrac{3}{2})/P(\tfrac{5}{2})/P(\tfrac{7}{2}) = 20.2\%/15.8\%/9.5\%/4.5\%, \tag{9}$$

(b) For $J = \frac{5}{2}$:

$$P(\tfrac{1}{2})/P(\tfrac{3}{2})/P(\tfrac{5}{2}) = 22.2\%/17.4\%/10.4\%, \tag{10}$$

(c) For $J = \frac{3}{2}$:

$$P(\tfrac{1}{2})/P(\tfrac{3}{2}) = 28.1\%/21.9\%. \tag{11}$$

Although the Gaussian distribution (9) tallies with the asymptotic experimental results (7), it will be noted that the Gaussian distribution (10) differs from the relative values cited above for the 440-keV ($\frac{5}{2}^+$) state.

The findings for ^{23}Na bear comparison with other recent findings of trends in substate population systematics. Thus, Rogers[48] has published results for the ^{19}F$(n,n'\gamma)$ reaction in which the 197-keV ($\frac{5}{2}^+$) level was fed by scattering of 1.3- and 2.56-MeV neutrons; his observed 197-keV pure $E2$ deexcitation γ transition distributions indicated the feeding to be in the ratio

$$P(\tfrac{1}{2})/P(\tfrac{3}{2})/P(\tfrac{5}{2}) = \begin{cases} 25\%/17\%/8\% & \text{at } E_n = 1.3 \text{ MeV}, \\ 18\%/22\%/10\% & \text{at } E_n = 2.56 \text{ MeV}, \end{cases} \tag{12}$$

while CN calculations gave

$$\begin{aligned} &24\%/18\%/8\% \quad \text{at } E_n = 1.3 \text{ MeV}, \\ &26\%/17\%/7\% \quad \text{at } E_n = 2.56 \text{ MeV}, \end{aligned} \tag{13}$$

and DI calculations gave

$$\begin{aligned} &29\%/21\%/0\% \quad \text{at } E_n = 1.3 \text{ MeV}, \\ &26\%/24\%/0\% \quad \text{at } E_n = 2.56 \text{ MeV}. \end{aligned} \tag{14}$$

Although the 197-keV level excitation function indicated the likelihood of some incoherent DI admixture, the substate populations and γ-ray angular distributions were indicative of a CN mechanism (note that the statistical assumption is even less likely to hold for ^{19}F than for ^{23}Na under these circumstances).

The only other instance in which the energy dependence of substate populations has up to the present been determined[23] is provided by the findings for the ^{55}Mn$(n,n'\gamma)$ reaction, which displayed the features indicated in Figs. 23 and 24. A comparison of Fig. 23 [for the substates of the 126-keV ($\frac{7}{2}^-$) first excited level of ^{55}Mn] with Fig. 22 [for the 2078-keV ($\frac{7}{2}^+$) second level of ^{23}Na] immediately shows the marked difference in structure, even though the monotonic diminution of $P(M)$ with increasing M remains preserved. Two sets of ^{55}Mn

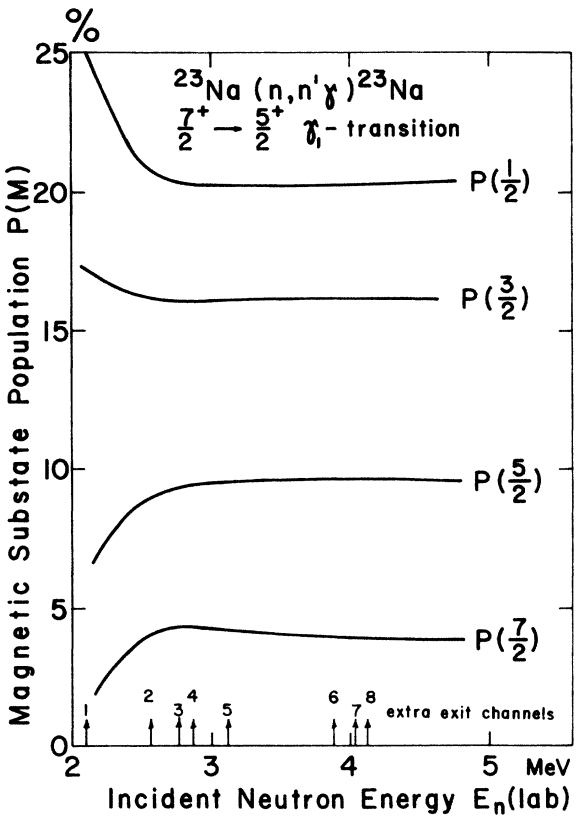

FIG. 22. Variation of CN theoretical magnetic substate populations of the 2078-keV ($\frac{7}{2}^+$) second level in ^{23}Na with energy. Note the threshold effect, evident also in the DI predictions cited in the text. The monotonic $P(M)$ sequence with M is preserved, and closely approximates a Gaussian distribution in this case. The population values derived from a least-squares Legendre fitting procedure applied to the experimental results proved to be unphysical (see discussion in text).

deexcitation γ-ray angular distribution measurements by Correia *et al.*[49] for incident energies E_n = 1.20 and 2.10 MeV permitted the extraction of least-squares-fit Legendre-polynomial coefficients, but unfortunately the multipole mixing ratio δ for this supposedly $M1/E2$ transition is not known and hence no conclusive determination of experimental populations $P(M)$ is feasible. However, on taking $\delta = 0$ (i.e., pure $M1$) as a specimen value for this parameter, quite reasonable agreement between experiment and theory ensues at the lower energy (1.20 MeV)—a possible fortuitous agreement as it worsens at the higher energy (2.10 MeV). At E_n = 3.0 MeV (an energy arbitrarily selected for purposes of comparison) the theoretical populations for this $\frac{7}{2}^-$ level in ^{55}Mn are in the ratio

$$P(\tfrac{1}{2})/P(\tfrac{3}{2})/P(\tfrac{5}{2})/P(\tfrac{7}{2}) = 13.3\%/13.0\%/12.3\%/11.3\%, \quad (15)$$

a result more evenly distributed than the values (7) of population for the $\frac{7}{2}^+$ level in ^{23}Na at the same incident energy, or than the Gaussian distribution (9).

An instance of more dramatic threshold behavior is discernible in Fig. 24, which shows the theoretical substate populations for the 1528-keV ($\frac{3}{2}^-$) fourth excited state of ^{55}Mn, calculated from the a_ν^* coefficients for the $\frac{3}{2}^- \rightarrow \frac{5}{2}^-$ deexcitation γ-ray angular distribution, assuming a CN mechanism. Again, although experimental data by Correia *et al.*[49] are available, the multipole mixture is unknown and the arbitrary choice of $\delta = 0$ (i.e., pure $M1$) yields $P(M)$ values that stand in only fair agreement with the theoretical predictions. Neither the experimental nor the theoretical values at E_n = 3.4 MeV approximate to the Gaussian distribution $P(\frac{1}{2})/P(\frac{3}{2}) = 26\%/24\%$ obtained from Eq. (8) with σ = 2.9: The theoretical curves at that point have already attained their "asymptotic" trend of population equality $[P(\frac{1}{2}) = P(\frac{3}{2}) = 25\%]$ beyond about E_n = 3 MeV.

As there is every reason to expect the statistical compound-nucleus model to furnish a valid description of neutron scattering characteristics for the medium-heavy target nucleus ^{55}Mn, the contrast with the findings for the much lighter nuclide ^{23}Na offers interesting comparisons. The desirability of pursuing further studies of magnetic substate populations along these lines under a variety of conditions in order to ascertain systematic trends is very evident.

VII. CONCLUSIONS

It is remarkable that under the conditions of the present measurements, which clearly fall short of meeting the requirements of the statistical continuum assumption inherent in conventional compound-nuclear scattering theory (note that the Gil-

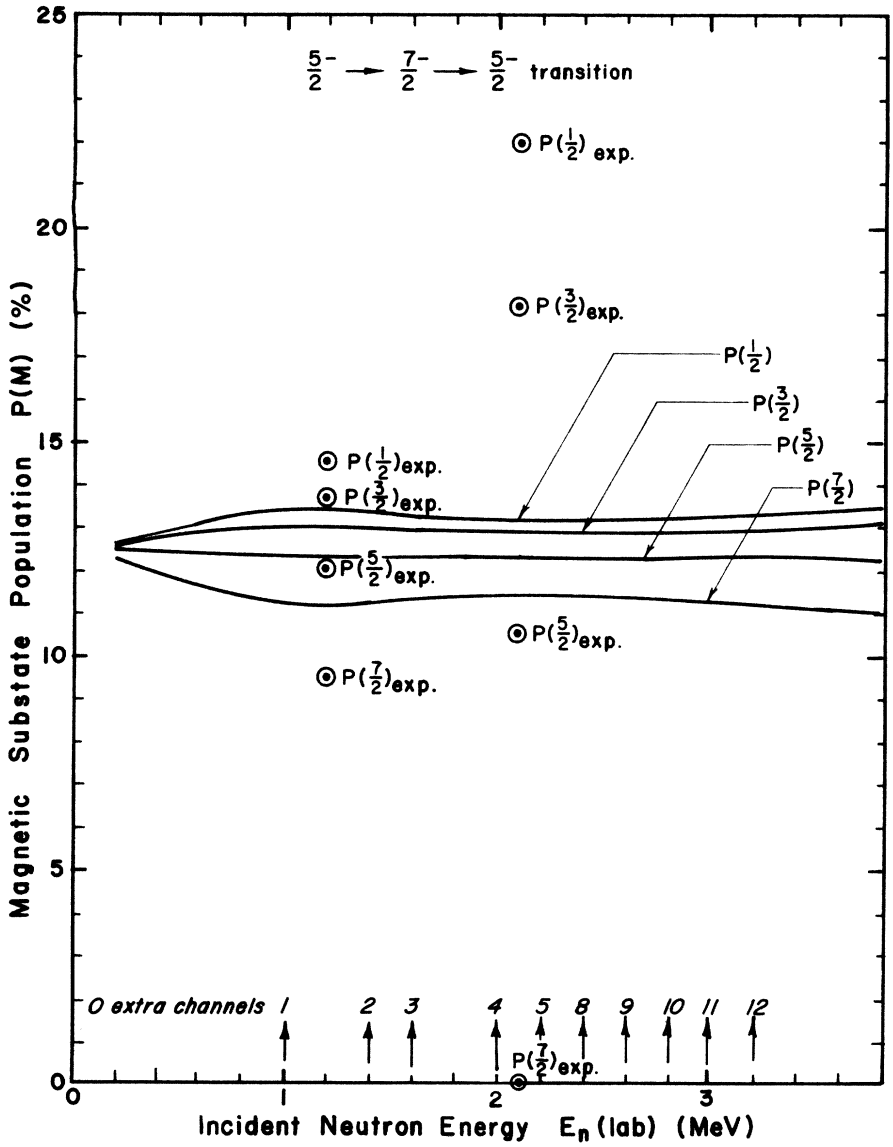

FIG. 23. Variation of CN theoretical substate populations $P(M)$ with incident neutron energy in $(n,n'\gamma)$ scattering leading to deexcitation of the 126-keV ($\frac{7}{2}^-$) first level of ^{55}Mn. The vacillating portion in the threshold region is distinctly less energy dependent than the ^{23}Na counterparts (cf. Fig. 22). Of two sets of experimental results deduced (Ref. 23) from data by Correia *et al.* (Ref. 49) at incident energies $E_n = 1.20$ and 2.10 MeV, the first yield fair agreement with CN theory when $\delta = 0$ (pure $M1$ multipolarity) is assumed (in the absence of explicit knowledge of the $M1/E2$ multipole mixing ratio δ), whereas the second set displays greater alignment [i.e., $P(M)$ differentiation] than the theory would predict.

bert-Cameron[47] level-density formula indicates that at $E_n = 0.5$ MeV the mean level spacing in ^{23}Na, for all spins and parities, is 50 keV, and for $E_n = 4.0$ MeV, it has diminished only to 10 keV), a reasonably good account of the experimental findings is nonetheless offered by CN theory. The DI formalism fails, even at the higher energies where discrepancies from the CN prediction develop more strongly, to render agreement with experimental values of total cross sections, differential cross sections, Legendre coefficients, and magnetic substate populations.

Only a few comparisons of our measured values with those of other authors can be made. The low-energy region of our excitation function for the 440-keV first level (Fig. 8) accords well with those presented by earlier investigators[8-10] and is compatible with more recent high-energy excitation

data by Lachkar *et al.*[11] at 6.3–8.8 MeV and by Dickens[50] at commensurate energies. In the angular distribution results for the 440-keV deexcitation γ radiation at $E_n = 1.50$ MeV (presented in the lower part of Fig. 15) we have included a set of values as measured by Towle and Gilboy (see Fig. 9 of Ref. 10), which stand in pronounced disagreement with our findings and, moreover, with CN and DI predictions. The curvature of their results is in the wrong sense, and the Legendre coefficients derived therefrom are therefore of the wrong sign, as indicated in Table I. If these coefficients are used, with $\delta = +0.08$, to determine the relative magnetic substate populations, one ob-

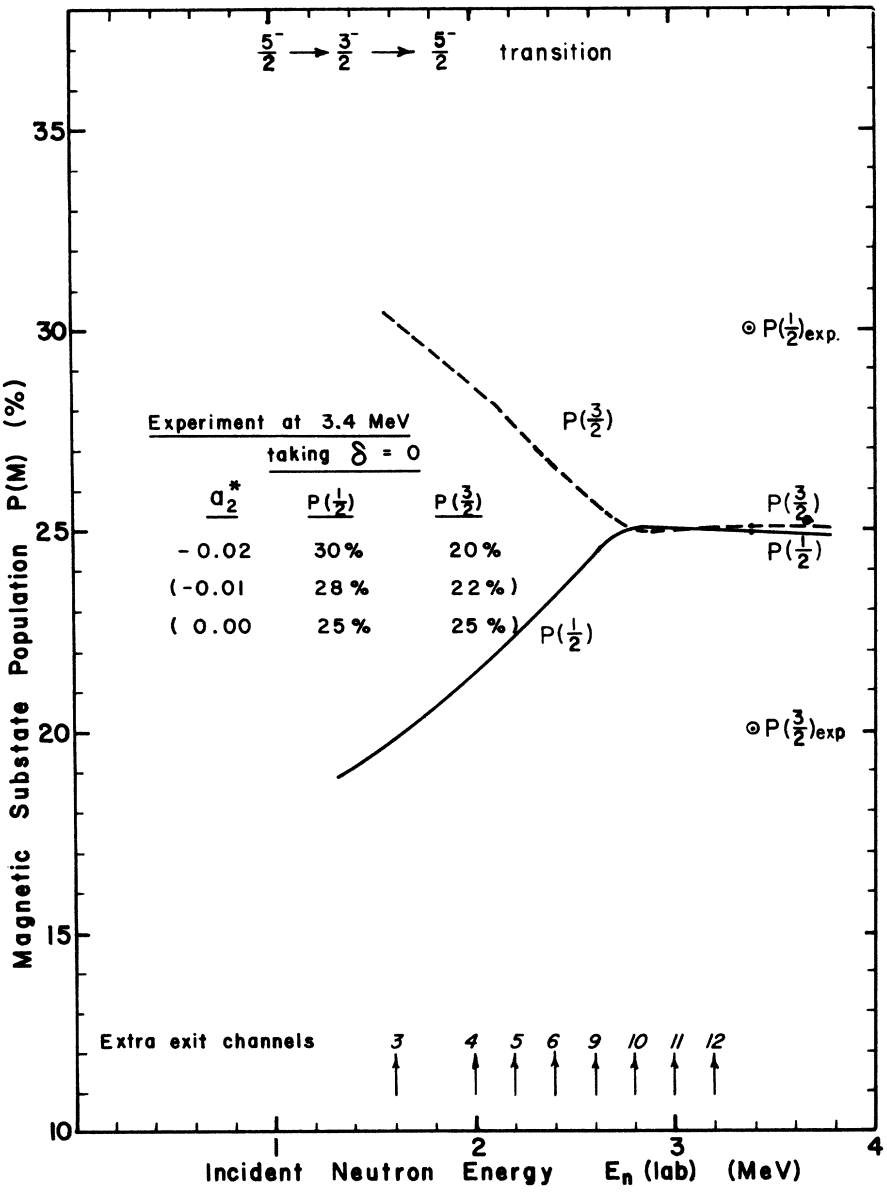

FIG. 24. The same as Fig. 23, but for the feeding of the 1528-keV ($\frac{3}{2}^-$) fourth level of ^{55}Mn by neutron inelastic scattering. The experimental results (Ref. 23) for $E_n = 3.4$ MeV do not match the CN theoretical prediction of population equality behond $E_n = 2.6$ MeV, nor do they correspond to the Gaussian distribution for ^{55}Mn with a spin cut-off parameter (Ref. 47) taken as $\sigma = 2.9$, namely $P(\frac{1}{2})/P(\frac{3}{2}) = 26\%/24\%$ [cf. Eq. (11)]. However, agreement with theory would have ensued from distribution isotropy ($a_2^* = 0$) whereas the least-squares fit to the measured distribution indicates only very weak anistropy, $a_2^* = -0.02$, which is perfectly compatible with zero.

tains the result

$$P(\tfrac{1}{2})/P(\tfrac{3}{2})/P(\tfrac{5}{2}) = (5\pm 2)\%/(14\pm 1)\%/(31\pm 3)\%. \quad (16)$$

Aside from being in marked contradiction to the results that we depict in Fig. 21 and discuss in the text, these relative populations can be criticized as being monotonically *increasing* with M, whereas all past findings and Gaussian distributions would favor the decrease of $P(M)$ with increasing M. We therefore feel that greater reliance can be reposed in our data, which fill a gap in hitherto existing information on the ^{23}Na$(n,n'\gamma)$ reaction.

ACKNOWLEDGMENTS

The authors appreciatively acknowledge the use of experimental and computational facilities at the University of Lowell (formerly the Lowell Technological Institute) and at the Massachusetts Institute of Technology, the maintenance of efficient accelerator operation by Mr. Charles Connolly and members of the accelerator staff, the assistance rendered by colleagues and students in the nuclear accelerator group, the provision of research grants by the U. S. National Science Foundation, and the generous permission to use independently computed results by Dr. V. C. Rogers of Brigham Young University.

*Work performed under the auspices of the U. S. National Science Foundation under Grant ENG-7421835.

[1]D. R. Donati, Ph.D. thesis, Lowell Technological Institute, June, 1973 (unpublished).

[2]J. L. Fowler, in *Proceedings of the International Conference on the Interactions of Neutrons with Nuclei, Lowell, 6–9, July*, 1976, edited by E. Sheldon (U.S. E.R.D.A. Technical Information Center, Oak Ridge, 1976), CONF-760715-P1, p. 611.

[3]R. Avery, in *Nuclear Cross Sections and Technology, Conference Proceedings, Washington, D. C., 1975*, edited by R. A. Schrack and C. D. Bowman (National Bureau of Standards Special Publication NBS SP No. 425, 1975), Vol. I, p. 45.

[4]E. Sheldon and V. C. Rogers, Compt. Phys. Commun. 6, 99 (1973).

[5]W. Hauser and H. Feshbach, Phys. Rev. 87, 366 (1952).

[6]E. Sheldon, Rev. Mod. Phys. 35, 795 (1963).

[7]E. Sheldon and D. M. Van Patter, Rev. Mod. Phys. 38, 143 (1966).

[8]J. M. Freeman and J. H. Montague, Nucl. Phys. 9, 181 (1958/59).

[9]I. L. Morgan, Phys. Rev. 103, 1031 (1956); D. Lind and R. Day, Ann. Phys. 12, 485 (1961).

[10]J. Towle and W. B. Gilboy, Nucl. Phys. 32, 610 (1962).

[11]J. Lachkar, Y. Patin, and J. Sigaud, in *Neitronnaya Fisica, National Conference on Neutron Physics, Kiev, U.S.S.R., 28 May–1 June, 1973* (Institute of Physics and Power Engineering, Obninsk, USSR, 1974), Part III, p. 187.

[12]D. W. Braben, L. C. Green, and J. C. Willmott, Nucl. Phys. 32, 584 (1962).

[13]A. R. Poletti and D. F. H. Start, Phys. Rev. 147, 800 (1966).

[14]A. R. Poletti, J. A. Becker, and R. E. McDonald, Phys. Rev. C 3, 964 (1970).

[15]R. A. Lindgren, R. G. Hirko, J. G. Pronko, A. J. Howard, M. W. Sachs, and D. A. Bromley, Nucl. Phys. A180, 1 (1972).

[16]M. F. da Silva, S. Kossionides, and J. C. Lisle, Nucl. Phys. A168, 663 (1971).

[17]J. Gomez del Campo, D. E. Gustafson, R. L. Robinson, P. H. Stelson, P. D. Miller, J. K. Bair, and J. B. McGrory, Phys. Rev. C 12, 1247 (1975).

[18]G. G. Frank, R. V. Elliott, R. H. Spear, and J. A. Kuehner, Can. J. Phys. 51, 1155 (1973).

[19]B. B. Back, R. R. Betts, C. Gaarde, and H. Oeschler, Phys. Rev. C 13, 875 (1976).

[20]D. E. Gustafson, S. T. Thornton, T. C. Schweizer, J. L. C. Ford, Jr., P. D. Miller, R. L. Robinson, and P. H. Stelson, Phys. Rev. C 13, 691 (1976).

[21]D. R. Donati, S. C. Mathur, E. Sheldon, P. Harihar, and W. A. Schier, Bull. Am. Phys. Soc. 18, 649 (1973), Paper No. GH6.

[22]E. Sheldon and D. R. Donati, Bull. Am. Phys. Soc. 18, 649 (1973), Paper No. GH7.

[23]E. Sheldon, J. A. Correia, D. R. Donati, and W. A. Schier, in *Proceedings of the International Conference on the Interactions of Neutrons with Nuclei, Lowell, 6–9 July, 1976* (See Ref. 2), p. 1322.

[24]A. D. Hanson and J. L. McKibben, Phys. Rev. 72, 673 (1947).

[25]W. D. Allen, in *Fast Neutron Physics*, Part I, edited by J. B. Marion and J. L. Fowler (McGraw-Hill, New York, 1960), p. 361.

[26]S. J. Bame, Jr., E. Haddad, J. E. Perry, Jr., and R. K. Smith, Rev. Sci. Instrum. 28, 997 (1957).

[27]C. H. Johnson, in *Fast Neutron Physics* (see Ref. 25), p. 247.

[28]R. Hully, in Proceedings of the DECUS Spring Symposium, 1969 (unpublished), p. 105.

[29]V. Barnes, United Kingdom Atomic Energy Authority Program Report No. 834 (W), Windscale Works, Seascale, Cumberland, United Kingdom, 1968 (unpublished); see also IEEE Trans. Nucl. Sci. 15, No. 3 (1968).

[30]D. R. Donati and S. C. Mathur, Proceedings of the DECUS Spring Symposium, 1970 (unpublished) p. 41.

[31]D. R. Donati, Gamma Spectral Analysis (GASPAN) and Isotopic Identification (ISOID), Digital Equipment Company Report, Maynard, Massachusetts, 1970 (unpublished).

[32]E. Sheldon, S. Mathur, and D. Donati, Compt. Phys. Commun. 2, 272 (1971).

[33]E. Sheldon and R. M. Strang, Compt. Phys. Commun. 1, 35 (1969).

[34]J. P. Chien and A. B. Smith, Nucl. Sci. Eng. 26, 500 (1966).

[35]C. T. Hibdon, Phys. Rev. 124, 500 (1961).
[36]P. D. Kunz, University of Colorado (private communication).
[37]L. C. Biedenharn and M. E. Rose, Rev. Mod. Phys. 25, 729 (1953).
[38]H. J. Rose and D. M. Brink, Rev. Mod. Phys. 39, 306 (1967).
[39]W. R. Gibbs, V. A. Madsen, J. A. Miller, W. Tobocman, E. C. Cox, and L. Mowry, NASA Lewis Research Center Report No. E-2206, 1963 (unpublished); V. A. Madsen, Nucl. Phys. 80, 177 (1966).
[40]R. H. Bassel, R. M. Drisko, and G. R. Satchler, Oak Ridge National Laboratory Report No. ORNL-3240, 1962 (unpublished).
[41]G. R. Satchler, Nucl. Phys. 55, 1 (1964).
[42]V. C. Rogers, Brigham Young University (private communication).
[43]S. Devons and L. J. B. Goldfarb, in *Handbuch der Physik*, edited by S. Flügge (Springer, Berlin, 1957), Vol. 42, p. 362.
[44]A. R. Poletti and E. K. Warburton, Phys. Rev. 137, B595 (1965).
[45]M. Ferentz and N. Rosenzweig, Argonne National Laboratory Report No. ANL-5324, 1955 (unpublished).
[46]T. E. O. Ericson, Phil. Mag. Suppl. 9, No. 36, 425 (1960).
[47]A. Gilbert and A. G. W. Cameron, Can. J. Phys. 43, 1446 (1965).
[48]V. C. Rogers, Phys. Rev. C 9, 527 (1974).
[49]J. A. Correia, W. A. Schier, L. E. Beghian, G. C. Couchell, J. J. Egan, G. H. R. Kegel, R. V. LeClaire, and A. Mittler, Nucl. Phys. (to be published).
[50]J. K. Dickens, Nucl. Sci. Eng. 50, 98 (1973).